Flux Crystal Growth, Structure, and Optical

Properties of the New Germanium Oxysulfide

$La_4(GeS_2O_2)_3$

Hong Yan,^{1,2} Akihide Kuwabara,³ Mark D. Smith,⁴ Kazunari Yamaura,^{1,2} Yoshihiro Tsujimoto, *,1,2,4 Hans-Conrad zur Loye*,⁴

¹Research Center for Functional Materials, National Institute for Materials Science, 1-1 Namiki, Tsukuba, Ibaraki 305-0044, Japan

²Graduate School of Chemical Sciences and Engineering, Hokkaido University, North 13 West 8, Kita-ku, Sapporo 060-0808, Japan

³Nanostructures Research Laboratory, Japan Fine Ceramics Center, 2-4-1 Mutsuno, Atsuta, Nagoya 456-8587, Japan

⁴Department of Chemistry and Biochemistry, University of South Carolina, Columbia, South Carolina 29208, United States

*Corresponding authors:

Yoshihiro Tsujimoto (E-mail: <u>TSUJIMOTO.Yoshihiro@nims.go.jp</u>)

Hans-Conrad zur Loye (E-mail: zurloye@mailbox.sc.edu)

Keywords. flux crystal growth, oxysulfide, wide-gap insulator, germanium

Abstract

Single crystals of a new germanium oxysulfide $La_4(GeS_2O_2)_3$ were grown out of a $BaCl_2\text{-}CaCl_2$ eutectic flux and the crystal structure was determined via single-crystal X-ray diffraction. Ivorywhite $La_4(GeS_2O_2)_3$ crystallizes in the centrosymmetric space group R-3 with lattice constants of a = b = 16.8283(3) Å, and c = 8.4140(2) Å. $La_4(GeS_2O_2)_3$ exhibits complex three-dimensional anion order in the framework composed of unusual GeS_2O_2 tetrahedra and three types of Lacentered polyhedra. Moreover, the triangular arrangement of the GeS_2O_2 tetrahedra around a columnar structure of alternating face-sharing LaO_{12} and LaS_6O_6 units resembles that of GeO_4 tetrahedra in the apatite germanate $La_{9,33}(GeO_4)_6O_2$, which features face-sharing LaO_9 columns. The combination of UV-Vis absorption measurements and first-principle calculations revealed the existence of an indirect optical band gap ($E_g = 3.67$ eV) between the valence band maximum composed of S 3p orbitals and the conduction band minimum composed of La 3d, La 4f, S 3p, and Ge 4s orbitals.

Introduction

Mixed-anion compounds, in which two or more anionic species are incorporated into one crystal structure, have provided a playground for solid-state chemists to explore unique properties. Differences in the essential characteristics of anions, i.e., ionic radius, electronegativity, oxidation state, and polarizability, often lead to short or long-range ordering of the anions, resulting in the formation of new anion sublattices and building blocks.¹⁻³ Mixed-anion structures containing oxide ions and different period 3–5 anions, such as oxide-sulfide and oxide-arsenide combinations, exclusively exhibit long-range anion ordering, particularly anion segregation in two dimensional (2D) layers.⁴⁻⁷ These anion segregations can be explained by the hard-soft acid-base (HSAB) theory,⁸ in which highly electronegative/polarizable cations prefer to bond with highly electronegative/polarizable anions. However, exceptions to the HSAB theory exist when differences in electronegativity (or polarizability) are small or when the concentration of a given anion is high compared to that of the other.

Oxychalcogenide compounds have been extensively studied because of their interesting optical properties. The incorporation of chalcogenide ions (*Ch*: S, Se, Te) into oxide sublattices raises the valence band maximum (VBM) and narrows the optical band gap, allowing for the tuning of the optical band gaps. ⁹⁻¹⁰ These band-gap engineered properties are useful for designing visible-light active photocatalysts, as observed in many layered oxysulfides ^{9,11-13}. The high polarizability of the chalcogenide ions also makes non-centrosymmetric oxychalcogenides promising non-linear optical materials exhibiting large second-harmonic generation (SHG) responses. Recently, our group reported a new polar zinc oxysulfide, SrZn₂S₂O, that crystallizes in the space group *Pmn*2₁ (no. 31) and that exhibited a large SHG response with phase matchability in contrast to non-phase-matching CaZnSO, space group *P6*₃*mc* (no. 186). ¹⁴⁻¹⁵ Moreover, SrZn₂S₂O was found

to be capable of reducing and oxidizing water under ultraviolet light irradiation with greater photocatalytic activity and photo-corrosion resistance than found for the mono-anionic Zn compounds, ZnO and ZnS.¹⁶ The structure of SrZn₂S₂O contains close-packed corrugated double layers of ZnS₃O tetrahedra that are present in two distinct orientations, in which sulfide and oxide ions form a unique 2D arrangement in the same layer. CaZnSO possesses a similar ZnS₃O building unit, however, the connectivities of these units differ: each of these two anions is isolated into separate 2D layers. Although the origins of the phase matchability and high photocatalytic activity in SrZn₂S₂O is not yet fully understood, it appears that the new anion-order design and arrangement of the anionic building blocks plays a crucial role in generating the unusual optical properties.

The flux crystal growth method has been recognized as a useful technique for synthesizing new mixed-anion compounds, most of which do not readily occur in single-crystal form.¹⁷⁻²⁰ In particular, alkali or alkaline earth halides, which can be easily removed with water, are widely used as fluxes for the synthesis of a wide range of new oxychalcogenides, including non-linear optical materials^{14,21}, low-dimensional magnets²²⁻²³, and superconductors²⁴. Following the discovery of SrZn₂S₂O, we applied this approach to develop new optical oxysulfide materials based on d^{10} metal-centered tetrahedra. Herein, we report the flux crystal growth of the new germanium-containing oxysulfide La₄(GeS₂O₂)₃ from a BaCl₂-CaCl₂ eutectic mixture. Its crystal structure, characterized by unusual GeS₂O₂ tetrahedra, electronic structure, and optical properties, are discussed.

Experimental

Synthesis. Single crystals of La₄(GeS₂O₂)₃ were grown out of a eutectic BaCl₂/CaCl₂ flux. First, 0.5 mmol of La₂S₃ (Alfa Aesar 99%), 1.0 mmol of GeO₂ (Rare Metallic 99.99%), 3.13 mmol of BaCl₂ (Rare Metallic 99.99%), and 3.13 mmol of CaCl₂ (Rare Metallic 99.99%) were loaded into a magnesia crucible in an Ar-filled glovebox. The crucible was sealed inside a silica tube that was evacuated to 10^{-4} Pa. The tube containing the starting materials was heated in a muffle furnace to 800 °C at 150 °C/h, held for 24 h, cooled to 500 °C at 5 °C/h, and then cooled to room temperature by turning the heater off. The product was washed in sonicated water and extracted from the flux. Ivory-white block La₄(GeS₂O₂)₃ crystals, along with colorless transparent platelet LaOCl crystals, were collected via vacuum filtration. The typical dimensions of the La₄(GeS₂O₂)₃ single crystals were $0.3 \times 0.3 \times 0.3$ mm³ (Figure 1). Elemental analysis by energy-dispersive X-ray spectroscopy (EDS) indicated a La:Ge:S atomic ratio of approximately 4.0:2.9:5.4, which is consistent with the chemical composition of the germanium oxysulfide phase. The crystal structure of La₄(GeS₂O₂)₃ was determined via single-crystal X-ray diffraction.

Single crystal structure determination. X-ray intensity data from a yellowish block crystal were collected at 301(2) K using a Bruker D8 QUEST diffractometer equipped with a PHOTON-100 CMOS area detector and an Incoatec microfocus (Mo K α radiation, λ = 0.71073 Å). The data collection covered 100% of the reciprocal space to $2\theta_{max}$ = 72.6°, with an average reflection redundancy of 14.7 and R_{int} = 0.057 after absorption correction. The raw area-detector data frames were reduced and corrected for absorption effects using the SAINT+ and SADABS programs.²⁵ ²⁶ Final unit cell parameters were determined by least-squares refinement of 9908 reflections taken from the data set. An initial structural model was obtained using SHELXT.²⁷

Subsequent difference Fourier calculations and full-matrix least-squares refinement against F^2 were performed with SHELXL-2018 using the ShelXle interface. ²⁸

Powder X-ray diffraction. Single crystals of La₄(GeS₂O₂)₃ were crushed with an agate mortar and pestle to obtain fine powders for collecting synchrotron X-ray powder diffraction (SXRD) patterns and UV-Vis diffuse reflectance spectra. SXRD measurements were performed at room temperature using a one-dimensional detector installed on the NIMS BL15XU beamline at SPring-8 in Japan. The synchrotron radiation X-rays were monochromatized to a wavelength of 0.65298 Å. The powdered sample of La₄(GeS₂O₂)₃ was loaded into a glass capillary tube (internal diameter: 0.2 mm). The diffraction data were collected in 0.003° increments over the 2–60° range and analyzed by Rietveld refinement using the RIETAN-FP program.²⁹

UV-Vis diffuse reflectance spectra and SEM-EDS. Diffuse reflectance spectroscopy measurements were performed at room temperature using a Shimazu UV-2600 spectrophotometer equipped with an ISR-2600Plus integration sphere. The diffuse reflectance data were internally converted to absorbance by the instrument using the Kubelka-Munk function. Single crystals of La₄(GeS₂O₂)₃ were analyzed by energy dispersive X-ray spectroscopy (EDS) equipped with a scanning electron microscopy (TESCAN Vega-e SBU). All crystals were mounted on carbon tape, and the analysis was carried using an accelerating voltage of 20 kV.

Density functional theory calculations.

To be described by Kuwabara san.

First-principles total energy calculations of La₄(GeS₂O₂)₃ were performed using the projector augmented wave method³⁰⁻³¹ as implemented in the Vienna Ab-initio Simulation Package (VASP).³²⁻³⁴ In the present study, the cut-off energy for the plane wave basis was 550 eV. The

exchange-correlation electron interaction potentials were considered via PBEsol-type generalized gradient approximation (GGA).³⁵

Results and discussion

The single-crystal structure analysis revealed that La₄(GeS₂O₂)₃ crystallizes in the space group R-3 (no. 148) with lattice constants of a = b = 16.8283(3) Å and c = 8.4140(2) Å. No significant deviation from full occupancy was detected for any atom. Thus, their occupancies were fixed at unity at the final stage of the structure refinements. The details of the structural refinement are listed in Table 1. The crystallographic parameters, including the atomic coordinates and atomic displacement parameters, are summarized in Table 2; anisotropic displacement parameters are listed in Table 3.

Figure 2 shows the SXRD patterns collected from a powder sample obtained by finely grinding hand-picked single crystals of La₄(GeS₂O₂)₃. The structural model determined by the single-crystal structure analysis was used for the Rietveld refinement. The calculated pattern well reproduced the observed patterns as the refinement readily converged with good reliability indexes, $R_{wp} = 4.90\%$, $R_B = 6.88\%$, and $R_F = 3.78\%$. Table S1 summarizes the final refined crystallographic data.

As shown in Figure 3, La₄(GeS₂O₂)₃ crystallizes in a unique three-dimensional crystal structure consisting of La- and Ge-centered polyhedra. Three crystallographically non-equivalent La1, La2, and La3 atoms occupy 18f, 3b, and 3a Wyckoff positions, respectively; in contrast, there is only one single germanium site occupying the 18f position. Two anions, namely O²⁻ and S²⁻, are fully ordered in the structure. Figure 4 shows the local coordination environments around the La

and Ge atoms. Of these three lanthanum sites, La1 and La2 are surrounded by two different anions. La1 is coordinated by three oxygen atoms at and average distance of $d_{\text{La-O1, La-O2}} \sim 2.45 \text{ Å}$ and six sulfur atoms at an average distance of $d_{\text{La-S1}} \sim 2.99$ Å and $d_{\text{La-S2}} \sim 3.28$ Å, forming a distorted gyroelongated square pyramid. Although these bond distances vary within 7 to 12% of the reference values derived from Shannon's ionic radii³⁶, the bond-valence-sum (BVS) calculation³⁷ for La1 yielded 2.91, which is consistent with the nominal oxidation state of the lanthanum ions. La2 is icosahedrally coordinated by six oxygen atoms at $d_{\text{La-O1}} = 2.6123(19) \text{ Å}$ and six sulfur atoms at $d_{\text{La-S2}} = 3.4262(6)$ Å. The La–O1 bond distance is 5% shorter than that of La-S2, but the La-S2 bond distance is 7% longer than the sum of the ionic radii of La³⁺ and O²⁻ /S²-. In contrast to these two lanthanum atoms, La3 is 12-fold coordinated with only oxygen atoms, forming a relatively symmetric icosahedron ($d_{La-O1} = 2.7159(19)$ Å, $d_{La-O2} = 2.7524(16)$ Å). The bond distances between lanthanum and oxygen atoms agree well, as they are within 1% of the sum of their ionic radii. The BVS values calculated for La2 and La3 were 2.54 and 2.63, respectively, much lower than the expected values. Typically, a BVS value lower than the ideal valence is often interpreted as indicating the existence of underbonding (or tensile stress) between the metal center and the surrounding ligands. However, this understanding is not applicable to the bond distances determined by XRD analysis. However, the reason for the low BVS values for La2 and La3 remains unclear. The germanium atom was tetrahedrally coordinated by two oxygen atoms at $d_{Ge-O1} = 1.7721(15)$ Å and $d_{Ge-O2} = 1.7908(18)$ Å and two sulfur atoms at $d_{\text{Ge-S1}} = 2.1600(10)$ Å and $d_{\text{Ge-S2}} = 2.1707(7)$ Å. These bond distances are consistent with those calculated from the sum of Ge⁴⁺ and La³⁺ ionic radii with O²⁻ and S²⁻ ionic radii, and the BVS calculation for Ge gave a reasonable value of 4.15. The S-Ge-S bond angle

of 124.56(3)° is much larger than the O–Ge–O bond angle of 99.89(8)°. This can be rationalized by considering the electrostatic repulsion between the sulfide ions with the larger ionic radii.

Germanium ions coordinated tetrahedrally by two sulfide and two oxide ions are rare compared to GeS_3O tetrahedra, which is often stabilized in oxysulfides having the melilite structures[ref]. To the best of our knowledge, only two other germanium-based compounds with a similar coordination geometry around the Ge center have been synthesized: $Na_2GeS_2(OH)_2\cdot_5H_2O^{38}$ and $AGeS_2O$ (A = Sr, Ba)²¹. The Ge–S and Ge–O distances and the S-Ge-S and O-Ge-O bond angles of these compounds are similar to those in $La_4(GeS_2O_2)_3$ (Table S2), but the GeS_2O_2 tetrahedron in $Na_2GeS_2(OH)_2\cdot_5H_2O$ is slightly elongated with smaller S–Ge–S and O–Ge–O bond angles.

Figure 5 shows the linkage between the La- and Ge-centered polyhedra. La2S₆O₆ and La3O₁₂ polyhedra share a common O₃ face to form one-dimensional (1D) chains along the *c* direction. Each La-based 1D chain is surrounded by La1S₆O₃ and GeS₂O₂ polyhedra in a complex manner. The La2S₆O₆ icosahedron are connected to six La1S₆O₃ polyhedra and six GeS₂O₂ tetrahedra by edge-sharing through pairs of oxygen and sulfur atoms. These La1-based polyhedra are separated by Ge and La2 atoms. In contrast, the La3O₁₂ icosahedron shares O₃ faces with six La1S₆O₃ polyhedra and O₂ edges with six GeS₂O₂ tetrahedra, both of which have two different independent *z* coordinates. Moreover, these six La1S₆O₃ polyhedra are linked with each other by sharing edges formed by a pair of oxygen and sulfur atoms. All GeS₂O₂ tetrahedra share edges with La1S₆O₃ and La3O₁₂/La2S₆O₆ polyhedra.

It is interesting to compare the present oxysulfide with the germanium oxyapatite $La_{9,33}(GeO_4)_6O_2$ that forms in the hexagonal space group $P6_3/m$. Despite the long-range anion-ordered structure and the completely different chemical composition of $La_4(GeS_2O_2)_3$, the

oxysulfide phase of this compound exhibits Ge- and La-centered polyhedra arrangements similar to those found in the oxyapatite structure. As shown in Figure 7, the La2O₉ polyhedra in the structure of La_{9,33}(GeO₄)₆O₂ form an infinite 1D chain along the *c* direction by sharing their common O₃ faces as in La₄(GeS₂O₂)₃. Moreover, these 1D chains are surrounded by six GeO₄ tetrahedra and six La1O₇ polyhedra with two different *z* coordinates, which are linked with La1O₇ through shared oxygen edges and vertexes, respectively. In both La₄(GeS₂O₂)₃ and La_{9,33}(GeO₄)₆O₂, the La2/La3 atoms are in the geometric center of the regular triangles formed by the Ge or La1 atoms. However, the Ge- or La1-based triangles form a regular hexagon in the oxysulfide, as seen in the top-down view of these crystal structures shown in Figure 6; this is in contrast with the distorted hexagon in the oxyapatite structure.

Figure 8 shows the UV-Vis absorption spectrum of a powdered La₄(GeS₂O₂)₃ sample. The absorption data were obtained by converting the sample's reflectance spectrum using the Kubelka-Munk transformation.⁴¹ The absorption curve presents two steep increases near 2.5 eV and 3.5 eV, and the corresponding absorption edge energies, which were estimated by extrapolating the linear portions of the absorption curve to the x axis, were $E_{g1} = 2.23$ eV and $E_{g2} = 3.67$ eV, respectively. Given that the sample is ivory-white, the absorption at E_{B1} is probably due to defects from anion vacancies, although the XRD analysis could detect neither anion nor cation vacancies. The larger absorption edge at E_{G2} should correspond to the intrinsic optical band gap, which will be discussed below.

First-principles calculations were performed to gain a better understanding of the relationship between the electronic structure and optical properties of La₄(GeS₂O₂)₃. Figure 9 shows the total and partial density of states (DOS) and the band dispersions of the oxysulfide compound. The total DOS reveals an energy gap with $E_g = 4.04 \text{ eV}$, which is close to the E_{g2} value but

significantly larger than the $E_{\rm g1}$ value. This result strongly suggests that the absorption edge observed at $E_{\rm g2}$ is intrinsic to the electronic structure of the oxysulfide phase. The valance bands located between -6 and 0 eV are mainly derived from the O 2p and S 3p orbitals, which are weakly hybridized with the La 3p, 3d, and 4f orbitals. The S 3p bands dominate the upper energy region in the valence band maximum (VBM) compared with the O 2p bands in the lower energy region, as is often observed in oxyfluoride compounds. $^{9\cdot10\cdot42}$ The conduction band minimum (CBM) is mainly composed of La 3d and 4f, Ge 4s, and S 3p orbitals. The band dispersion shown in Figure 10 indicates that the VBM is located at point Γ and the CBM between points T and P. The optical absorption above $E_{\rm g2}$ in the UV-Vis spectrum results from the transition from the VBM to the CVM. The Ge 4s and 4p bands are located in the narrow energy regions between -8 and -7 eV and -6 and -4 eV, respectively, and are highly hybridized with O 2p and S 3p orbitals. The localized nature of these Ge bands is in contrast to the widely dispersive La bands located in the valence bands, resulting from the isolated linkages between GeS $_2$ O $_2$ tetrahedra.

Conclusion

A new germanium oxysulfide $La_4(GeS_2O_2)_3$ with an indirect optical band gap of 3.67 eV was synthesized from a $BaCl_2$ - $CaCl_2$ eutectic molten salt. Single-crystal structure analysis demonstrated a unique structure comprised of unusual GeS_2O_2 tetrahedra linked with La-centered polyhedra through corner or edge sharing. The linkage between the Ge- and La-centered polyhedra is similar to that observed in the germanium oxyapatite, $La_{9,33}(GeO_4)_6O_2$, although the oxysulfide phase does not possess the so-called "apatite channel" in which oxide ions at $(0\ 0\ z)$ are mobile at high temperatures. Recently, several new classes of sulfide materials have shown promise for practical use as solid-state electrolytes for Li-ion batteries. In the structures of such

materials, highly polarizable sulfur ions play an important role in promoting high Li-ion conductivity. In $La_4(GeS_2O_2)_3$, each $La1S_6O_3$ polyhedron is connected to sulfide ions by edge-sharing, resulting in the formation of the sulfide-rich regions outside the alternating chains of face-sharing LaO_{12} and LaS_6O_6 units. Future studies should seek to determine if this three-dimensional anion order in $La_4(GeS_2O_2)_3$ creates Li-ion pathways via the substitution of Li for La atoms, as found in the $La_{1,x}Li_yTiO_3$ perovskite⁴³.

ASSOCIATED CONTENT

Supporting Information.

The following files are available free of charge.

Rietveld refinement details, Selected bond distances and bond angles (PDF)

Crystallographic information (CIF)

AUTHOR INFORMATION

Corresponding Author

*Yoshihiro Tsujimoto. Email: <u>TSUJIMOTO.Yoshihiro@nims.go.jp</u>.

*Hans-Conrad zur Loye. E-mail: <u>zurloye@mailbox.sc.edu</u>.

Notes

The authors declare no competing financial interest.

ACKNOWLEDGMENT

We gratefully acknowledge a research grant from UofSC (NSF grant DMR-1806279). YT and AK acknowledge Grant-in-Aid for Scientific Research from Japan Society of for the Promotion

Science (JSPS) (no. 16H06438, 16H06439, 16H06440, 17H05493, 19H04711). KY acknowledges a research grant for Innovative Science and Technology Initiative for Security, from ATLA, Japan.

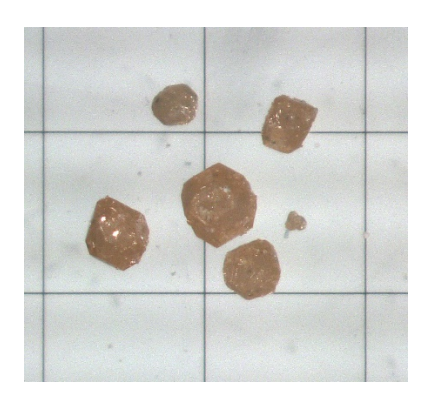


Figure 1. Photograph of single crystals of La₄(GeS₂O₂)₃ on a 1 mm grid-cell plate.

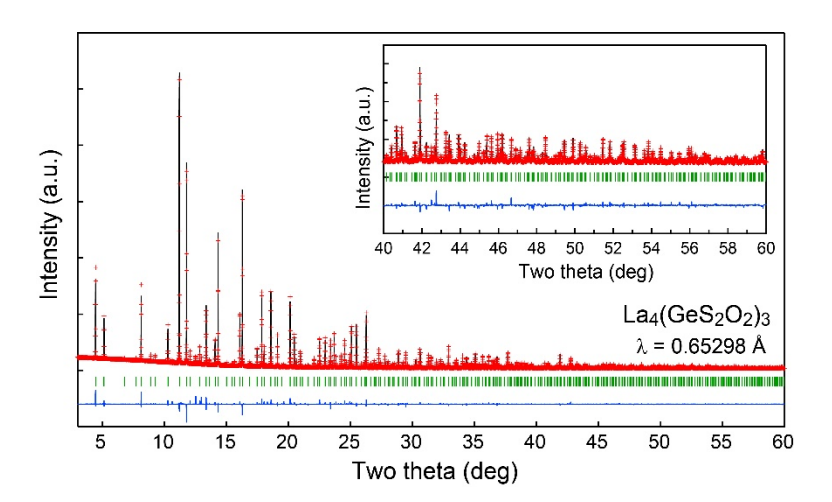


Figure 2. SXRD patterns of $La_4(GeS_2O_2)_3$ measured at room temperature. Obtained, calculated, and difference data are presented by cross marks (red), upper solid lines (black), bottom solid lines (blue), respectively. The vertical lines (green) represented the expected Bragg peak positions of $La_4(GeS_2O_2)_3$.

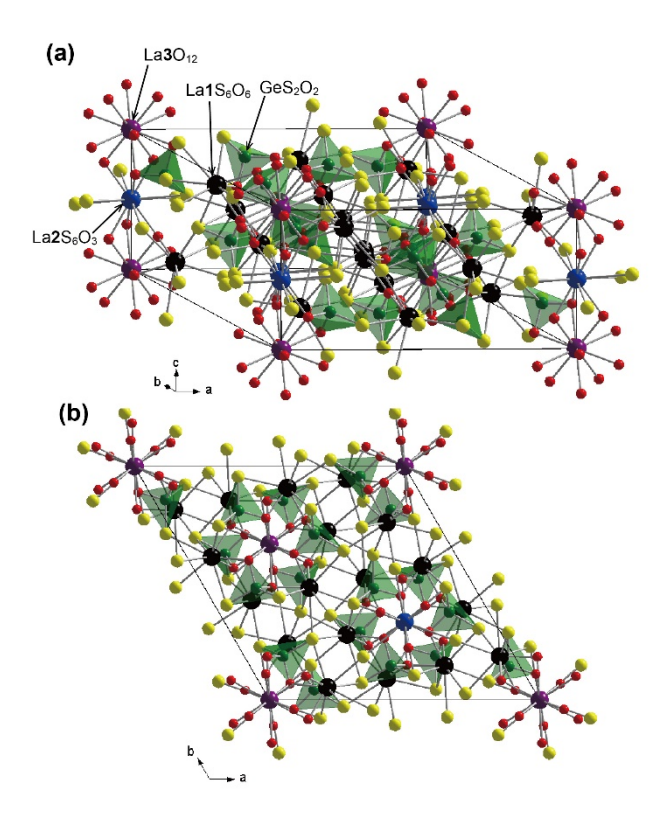


Figure 3. Crystal structure of $La_4(GeS_2O_2)_3$. Black, blue, purple, green, red, and yellow spheres stand for La1, La2, La3, Ge, O, and S atoms, respectively.

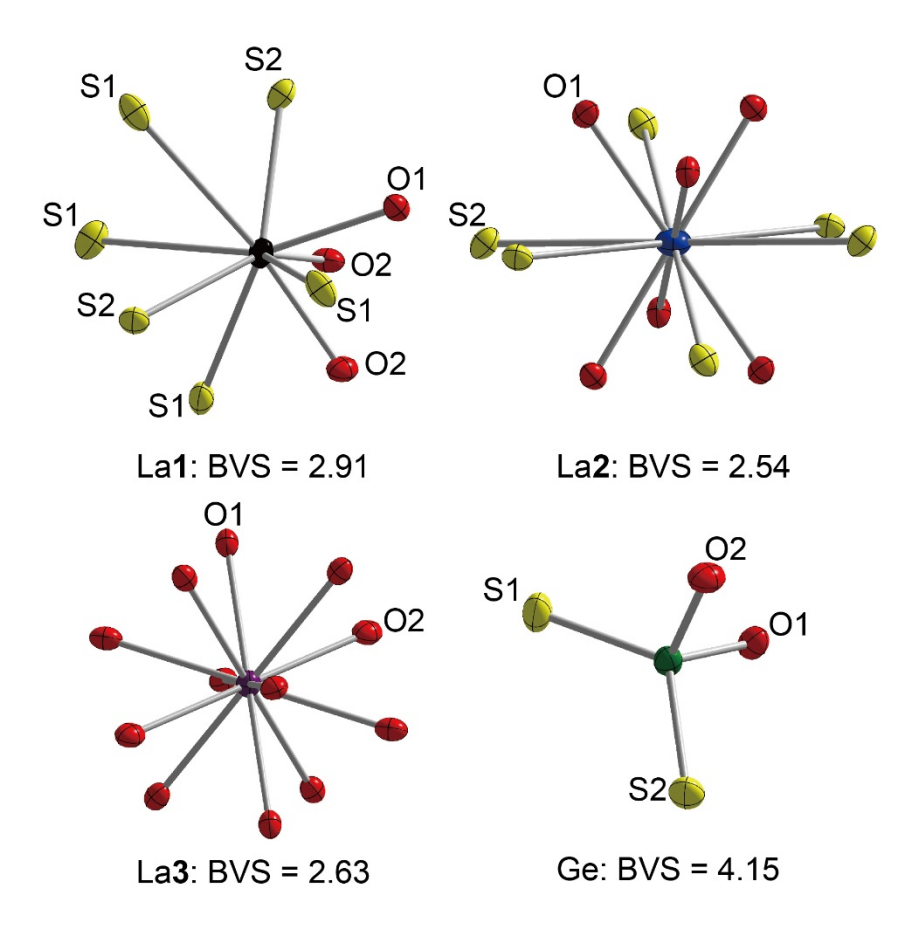


Figure 4. Local coordination environment around La1, La2, La3 and Ge atoms. Displacement ellipsoids are shown at the 90% level.

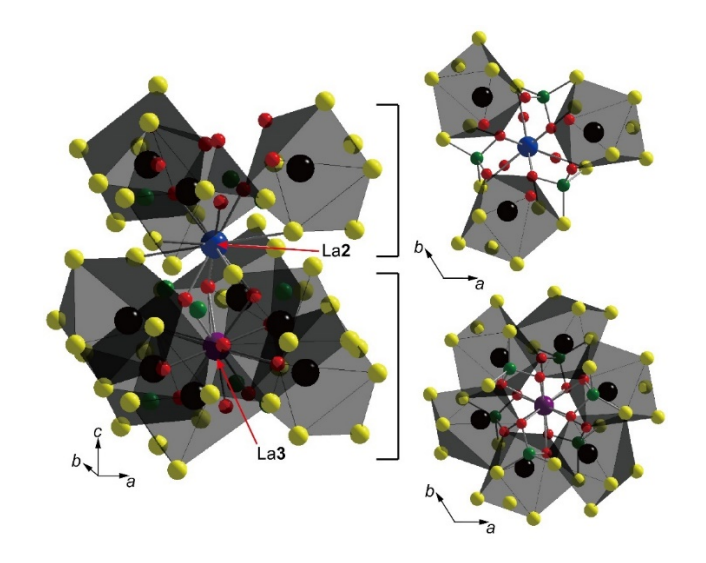


Figure 5. Linkage between La- and Ge-centered polyhedra in $La_4(GeS_2O_2)_3$ viewed along two different directions. La2 and La3-centered polyhedra are surrounded by six La1-centered polyhedra and six Ge-centered tetrahedra in a different arrangement.

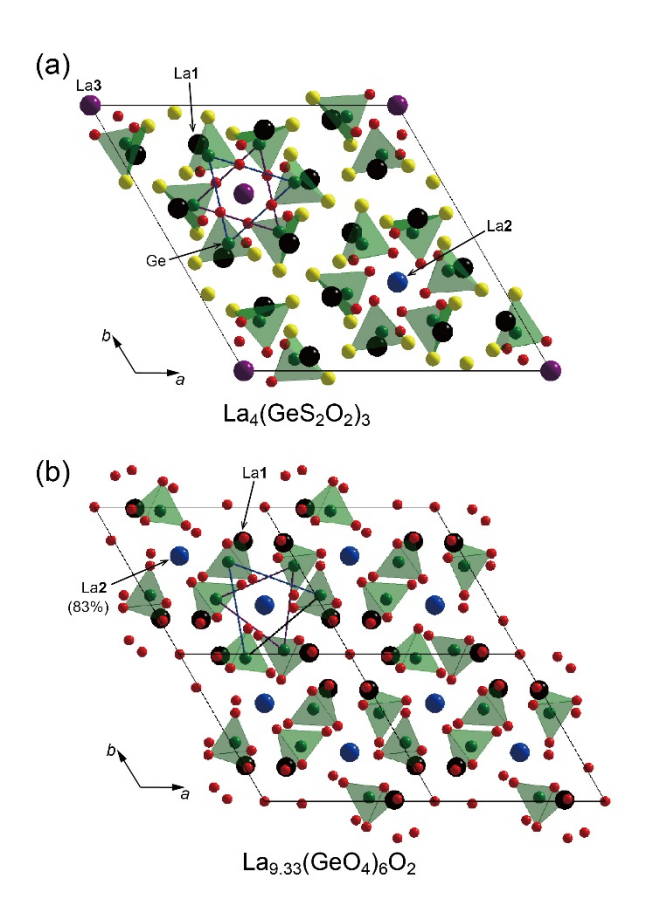


Figure 6. The crystal structure of $La_4(GeS_2O_2)_3$ (a) and $La_{9.33}(GeO_4)_6O_2$ (b) viewed along the c axis.

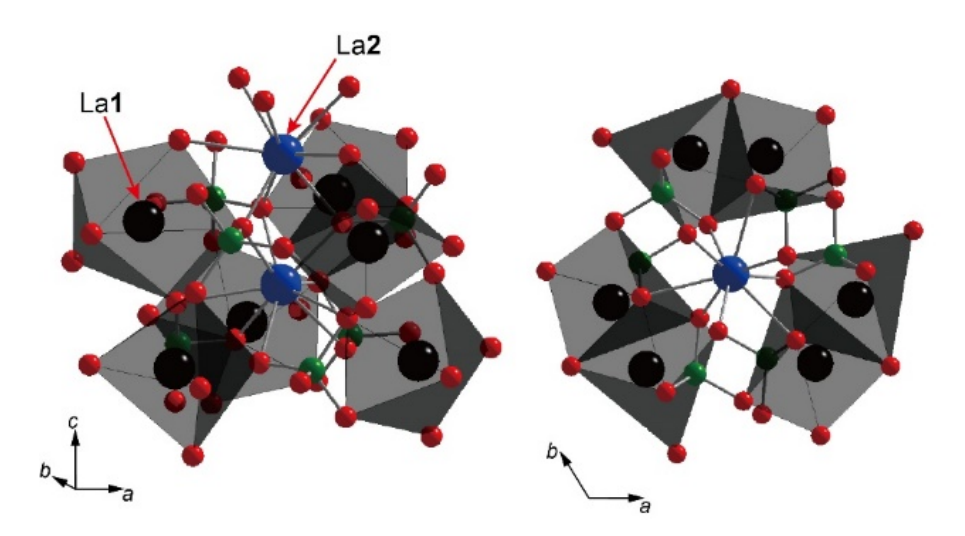


Figure 7. Linkage between La- and Ge-centered polyhedra in La_{9,33}(GeO₄)₆O₂ viewed along two different directions. La**2**-centered polyhedra are surrounded by six La**1**-centered polyhedra and six Ge-centered tetrahedra in a different arrangement.

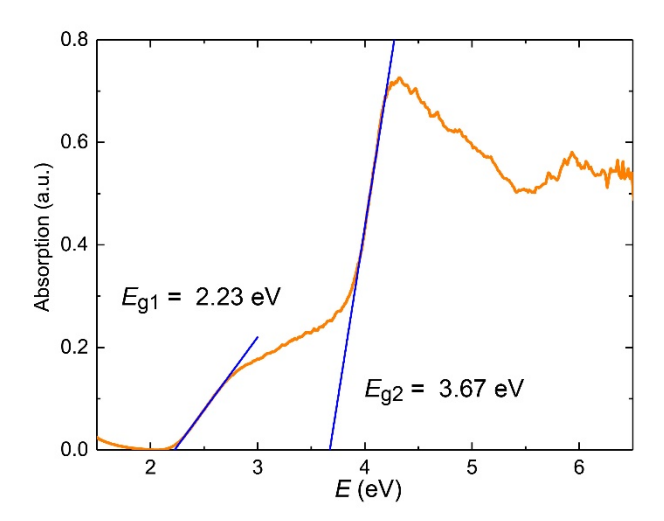


Figure 8. UV-vis optical absorption spectrum of La₄(GeS₂O₂)₃, which was converted from the diffuse reflectance data using the Kubelka- Munk function.

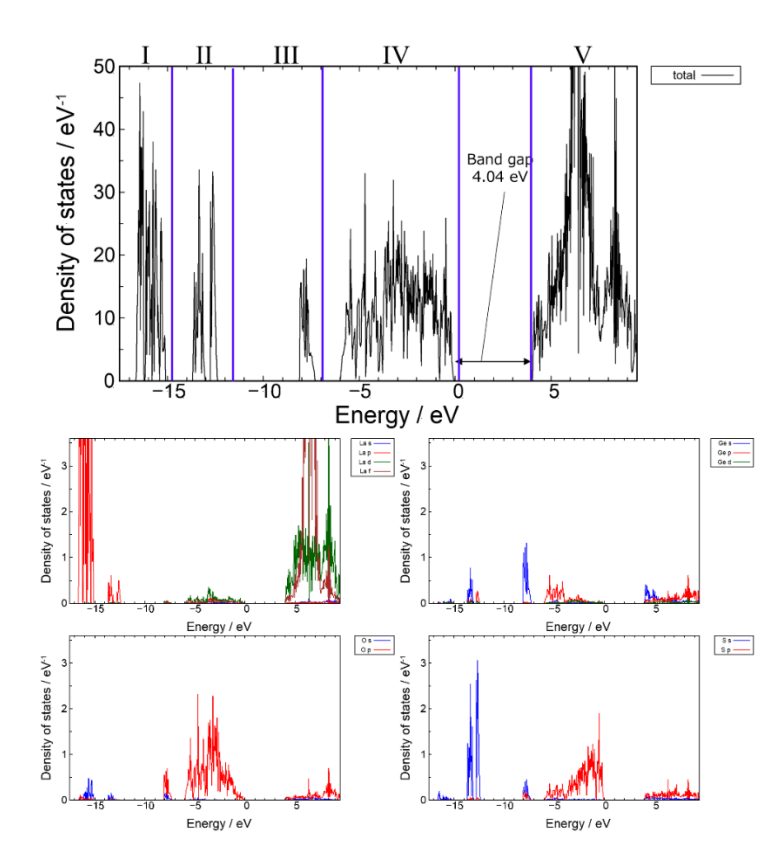


Figure 9. Total and partial density of states of $La_4(GeS_2O_2)_3$ obtained by first-principles calculations. (to be revised by Kuwabara san)

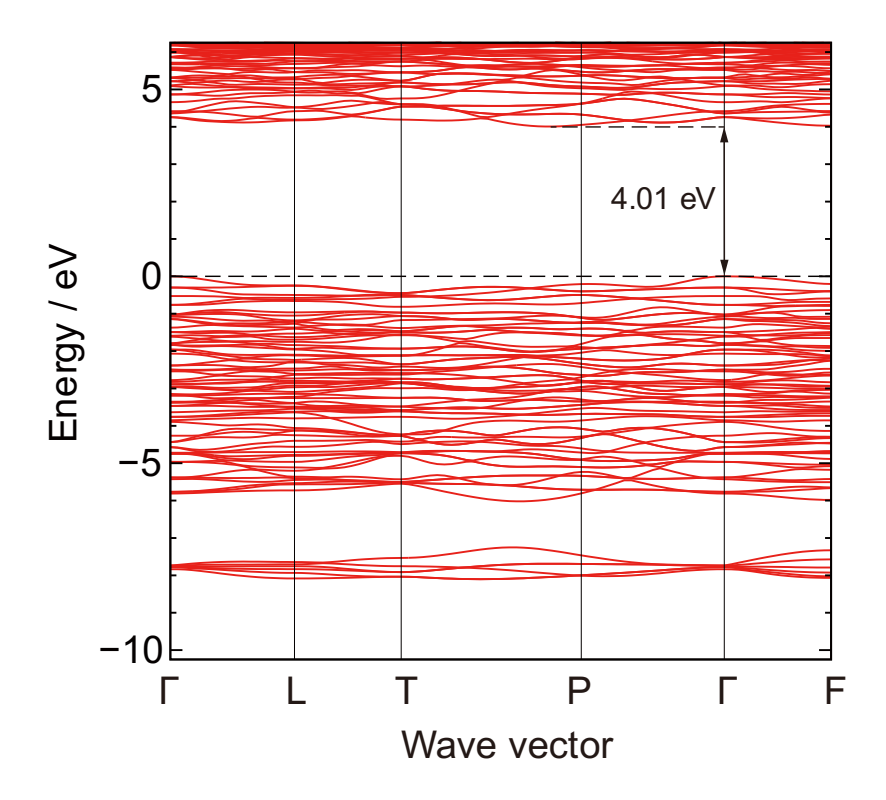


Figure 10. Band dispersion of La₄(GeS₂O₂)₃ obtained by first-principles calculations. (to be revised by Kuwabara san)

 $\begin{tabular}{ll} \textbf{Table 1.} Results of the Structure Refinement of $La_4(GeS_2O_2)_3$ Using Single-Crystal X-ray \\ Diffraction \end{tabular}$

Formula	$La_4(GeS_2O_2)_3$
Formula weight	1061.77
Radiation	Mo Kα (λ=0.71073Å)
T(K)	301(2)
Crystal system	trigonal
Space group	R-3
a (Å)	16.8283(3)
b (Å)	16.8283(3)
c (Å)	8.4140(2)

77 (9 2)	20.62.74(0)
$V(Å^3)$	2063.54(9)
Z	6
$D_{ m calc}$ (g/cm ³)	5.126
F_{000}	2808
no. of measured reflns	32798
no. of unique reflns	2225
no. of observed reflns	1868
$(F^2 > 2\sigma(F^2))$	1000
$R_{ m int}$ (%)	5.70
$R[F^2 > 2\sigma(F^2)]/wR(F^2)$ (%)	2.22/3.45
GoF	1.062

 $\label{eq:continuous_continuous$

atom	site	х	У	Z	Occp.	$U_{\rm eq}$ (Å ² ×10 ²)
La1	18 <i>f</i>	0.18672(2)	0.24104(2)	0.15890(2)	1	0.00902(3)
La2	3 <i>b</i>	0	0	1/2	1	0.01243(7)
La3	3 <i>a</i>	0	0	0	1	0.00792(6)
Ge	18 <i>f</i>	0.18713(2)	0.04347(2)	0.24397(3)	1	0.00720(5)
S 1	18 <i>f</i>	0.26044(4)	-0.02833(4)	0.19177(7)	1	0.01228(11)
S2	18 <i>f</i>	0.22741(4)	0.14889(4)	0.42442(7)	1	0.01035(11)
O1	18 <i>f</i>	0.06959(11)	-0.04136(11)	0.25780(19)	1	0.0082(3)
O2	18 <i>f</i>	0.18462(11)	0.10106(11)	0.06669(18)	1	0.0099(3)

Table 3. Anisotropic Displacement Parameters U_{ij} (Å²×10²) for La₄(GeS₂O₂)₃ at 301 K.

U_{11}	U_{22}	U_{33}	U_{23}	U_{13}	U_{12}
0.00858(6)	0.00651(6)	0.01144(6)	-0.00042(4)	-0.00159(5)	0.00338(5)
0.01475(10)	0.01475(10	0.00781(14)	0	0	0.00737(5)
0.00733(9)	0.00733(9)	0.00910(13)	0	0	0.00366(4)
0.00696(11)	0.00689(11	0.00789(10)	-0.00046(8)	-0.00042(8)	0.00356(9)
0.0096(3)	0.0139(3)	0.0158(3)	-0.0047(2)	-0.0019(2)	0.0077(2)
0.0099(3)	0.0099(3)	0.0106(2)	-0.00343(19)	-0.00225(19)	0.0046(2)
0.0068(7)	0.0071(7)	0.0096(7)	-0.0008(6)	0.0010(6)	0.0025(6)
0.0136(8)	0.0109(8)	0.0070(7)	0.0010(6)	0.0002(6)	0.0074(7)

Table S1. Atomic Coordinates and Isotropic Displacement Parameters $U_{\rm iso}$ Refined from SXRD Data Collected from La₄(GeS₂O₂)₃ at Room Temperature.

Atom	Site	х	у	z	Occp.a	$U_{\rm iso}$ (Å ² ×10 ²)
La1	18 <i>f</i>	0.18640(7)	0.24115(7)	0.15842(12)	1	0.780(15)
La2	3b	0	0	1/2	1	1.11(6)
La3	3a	0	0	0	1	0.43(4)
Ge	18 <i>f</i>	0.18670(9)	0.04372(13)	0.24143(17)	1	0.45(3)
S 1	18 <i>f</i>	0.2602(3)	-0.0272(2)	0.1898(4)	1	1.26(8)
S2	18 <i>f</i>	0.2273(2)	0.1531(2)	0.4181(4)	1	1.54(9)
O1	18 <i>f</i>	0.0679(5)	-0.0441(6)	0.2503(9)	1	0.18(14)b

O2 18f 0.1753(5) 0.0996(7) 0.0684(9) 1 0.18 b

The space group is R-3 (No. 148) with a = b = 16.82677(1) Å, c = 8.41591(1) Å. R indices are $R_{\rm wp} = 4.90\%$, $R_{\rm B} = 6.88\%$, $R_{\rm F} = 3.78\%$. ^a Site occupancy for each atom was fixed to unity. ^b The $U_{\rm iso}$ values for O1 and O2 atoms were constrained to the same value.

Table S2. Selected Interatomic Distances (Å) and Bond Angles (°) of La₄(GeS₂O₂)₃

	bond distance (Å)		bond angle (°)
La1-O1	2.473(2)	O2-La1-O2	73.36(6)
La1-O1	2.4228(19)	O2-La1-O1	73.67(5)
	2.464(3)	O2-La1-O1	74.01(5)
La1-S1	3.1571(7)	O1-La2-O1×6	65.62(6)
	3.2076(7)	O1-La2-O1×6	114.38(6)
	3.3468(7)	O1-La2-O1×2	180.000
	3.4280(8)	O1-La2-S2×4	61.99(4)
La1-S2	2.9877(8)	O1-La2-S2×6	118.01(4)
	2.9905(7)	O1-La2-S2×6	115.82(4)
La2-O1×6	2.6123(19)	O1-La2-S2×6	64.18(4)
La2-S2×6	3.4262(6)	O1-La2-S2×6	62.06(4)
La3-O1×6	2.7159(16)	O1-La2-S2×6	117.94(4)
La3-O2×6	2.7524(16)	S2-La2-S2×5	63.363(6)
Ge1-O1	1.7720(16)	S2-La2-S2×5	116.637(6)
Ge1-O2	1.7908(16)	S2-La2-S2×3	180.000
Ge1-S1	2.1600(6)	O1-La3-O1×6	117.18(5)
Ge1-S2	2.1701(6)	O1-La3-O1×6	62.82(5)
		O1-La3-O1×3	180.00(8)
		O1-La3-O2×6	120.17(5)

O1-La3-O2×6	65.81(5)
O1-La3-O2×6	114.19(5)
O1-La3-O2×6	59.83(5)
O2-La3-O2×6	115.95(2)
O2-La3-O2×6	64.05(2)
O1-Ge1-O2	99.89(7)
O1-Ge1-S1	106.40(5)
O2-Ge1-S1	107.94(5)
O1-Ge1-S2	112.29(5)
O2-Ge1-S2	102.86(5)
S1-Ge1-S2	124.56(2)

Reference

- 1. Kageyama, H.; Hayashi, K.; Maeda, K.; Attfield, J. P.; Hiroi, Z.; Rondinelli, J. M.; Poeppelmeier, K. R., Expanding frontiers in materials chemistry and physics with multiple anions. *Nat Commun* **2018**, *9* (1), 772.
- 2. Tsujimoto, Y.; Yamaura, K.; Takayama-Muromachi, E., Oxyfluoride Chemistry of Layered Perovskite Compounds. *Applied Sciences* **2012**, *2* (1), 206-219.
- 3. Keen, D. A.; Goodwin, A. L., The crystallography of correlated disorder. *Nature* **2015**, *521* (7552), 303-9.
- 4. Clarke, S. J.; Adamson, P.; Herkelrath, S. J.; Rutt, O. J.; Parker, D. R.; Pitcher, M. J.; Smura, C. F., Structures, physical properties, and chemistry of layered oxychalcogenides and oxypnictides. *Inorg Chem* **2008**, *47* (19), 8473-86.
- 5. <Zhu-1997-Crystal structure of new layered oxys.pdf>.
- 6. <Broadley-2005-Vertex-linked ZnO2S2 tetrahedra.pdf>.
- 7. Valldor, M., Anion Ordering in Bichalcogenides. *Inorganics* **2016**, *4* (3), 23.
- 8. Pearson, R. G., Hard and Soft Acids and Bases. *Journal of the American Chemical Society* **1963**, *85* (22), 3533-3539.
- 9. Goto, Y.; Seo, J.; Kumamoto, K.; Hisatomi, T.; Mizuguchi, Y.; Kamihara, Y.; Katayama, M.; Minegishi, T.; Domen, K., Crystal Structure, Electronic Structure, and Photocatalytic Activity of Oxysulfides: La2Ta2ZrS2O8, La2Ta2TiS2O8, and La2Nb2TiS2O8. *Inorg Chem* **2016**, *55* (7), 3674-9.
- 10. Yashima, M.; Ogisu, K.; Domen, K., Structure and electron density of oxysulfide Sm2Ti2S2O4.9, a visible-light-responsive photocatalyst. *Acta Crystallogr B* **2008**, *64* (Pt 3), 291-8.
- 11. Kabbour, H.; Sayede, A.; Saitzek, S.; Lefevre, G.; Cario, L.; Trentesaux, M.; Roussel, P., Structure of the water-splitting photocatalyst oxysulfide alpha-LaOInS2 and ab initio prediction of new polymorphs. *Chem Commun (Camb)* **2020**, *56* (11), 1645-1648.
- 12. Wang, Q.; Nakabayashi, M.; Hisatomi, T.; Sun, S.; Akiyama, S.; Wang, Z.; Pan, Z.; Xiao, X.; Watanabe, T.; Yamada, T.; Shibata, N.; Takata, T.; Domen, K., Oxysulfide photocatalyst for visible-light-driven overall water splitting. *Nat Mater* **2019**, *18* (8), 827-832.
- 13. Ogisu, K.; Ishikawa, A.; Teramura, K.; Toda, K.; Hara, M.; Domen, K., Lanthanum–Indium Oxysulfide as a Visible Light Driven Photocatalyst for Water Splitting. *Chemistry Letters* **2007**, *36* (7), 854-855.
- 14. Tsujimoto, Y.; Juillerat, C. A.; Zhang, W.; Fujii, K.; Yashima, M.; Halasyamani, P. S.; zur Loye, H.-C., Function of Tetrahedral ZnS3O Building Blocks in the Formation of SrZn2S2O: A Phase Matchable Polar Oxysulfide with a Large Second Harmonic Generation Response. *Chemistry of Materials* **2018**, *30* (18), 6486-6493.
- 15. Sambrook, T.; Smura, C. F.; Clarke, S. J.; Ok, K. M.; Halasyamani, P. S., Structure and physical properties of the polar oxysulfide CaZnOS. *Inorg Chem* **2007**, *46* (7), 2571-4.
- 16. Nishioka, S.; Kanazawa, T.; Shibata, K.; Tsujimoto, Y.; Zur Loye, H. C.; Maeda, K., A zinc-based oxysulfide photocatalyst SrZn2S2O capable of reducing and oxidizing water. *Dalton Trans* **2019**, *48* (42), 15778-15781.
- 17. Fjellvag, O. S.; Nygard, K. H.; Vajeeston, P.; Sjastad, A. O., Advances in the LiCl salt flux method and the preparation of phase pure La2-xNdxLiHO3 (0 </= x </= 2) oxyhydrides. *Chem Commun (Camb)* **2019,** *55* (26), 3817-3820.
- 18. Hosono, A.; Masubuchi, Y.; Yasui, S.; Takesada, M.; Endo, T.; Higuchi, M.; Itoh, M.; Kikkawa, S., Ferroelectric BaTaO2N Crystals Grown in a BaCN2 Flux. *Inorg Chem* **2019**.

- 19. Zhong, C.; Kato, D.; Takeiri, F.; Fujii, K.; Yashima, M.; Nishiwaki, E.; Fujii, Y.; Koreeda, A.; Tassel, C.; Abe, R.; Kageyama, H., Single Crystal Growth of Sillén–Aurivillius Perovskite Oxyhalides Bi4NbO8X (X = Cl, Br). *Inorganics* **2018**, *6* (2), 41.
- 20. Juillerat, C. A.; Moore, E. E.; Morrison, G.; Smith, M. D.; Besmann, T.; Zur Loye, H. C., Versatile Uranyl Germanate Framework Hosting 12 Different Alkali Halide 1D Salt Inclusions. *Inorg Chem* **2018**, *57* (18), 11606-11615.
- 21. Zhang, X.; Xiao, Y.; Wang, R.; Fu, P.; Zheng, C.; Huang, F., Synthesis, crystal structures and optical properties of noncentrosymmetric oxysulfides AeGeS2O (Ae = Sr, Ba). *Dalton Trans* **2019**.
- 22. Blandy, J. N.; Liu, S.; Smura, C. F.; Cassidy, S. J.; Woodruff, D. N.; McGrady, J. E.; Clarke, S. J., Synthesis, Structure, and Properties of the Layered Oxide Chalcogenides Sr2CuO2Cu2S2 and Sr2CuO2Cu2Se2. *Inorg Chem* **2018**.
- 23. Lei, H.; Ryu, H.; Ivanovski, V.; Warren, J. B.; Frenkel, A. I.; Cekic, B.; Yin, W.-G.; Petrovic, C., Structure and physical properties of the layered iron oxychalcogenide BaFe2Se2O. *Physical Review B* **2012**, *86* (19).
- 24. Nagao, M.; Miura, A.; Urushihara, D.; Maruyama, Y.; Goto, Y.; Mizuguchi, Y.; Moriyoshi, C.; Kuroiwa, Y.; Wang, Y.; Watauchi, S.; Asaka, T.; Takano, Y.; Tadanaga, K.; Tanaka, I., Flux Growth and Superconducting Properties of (Ce,Pr)OBiS2 Single Crystals. *Front Chem* **2020**, *8*, 44.
- 25. Krause, L.; Herbst-Irmer, R.; Sheldrick, G. M.; Stalke, D., Comparison of silver and molybdenum microfocus X-ray sources for single-crystal structure determination. *J Appl Crystallogr* **2015**, *48* (Pt 1), 3-10.
- 26. Bruker AXS, I., Madison, Wisconsin, USA, APEX3 Version 2016.5-0 and SAINT+ Version 8.37A. **2016**.
- 27. Sheldrick, G. M., Crystal structure refinement with SHELXL. *Acta Crystallogr C Struct Chem* **2015**, 71 (Pt 1), 3-8.
- 28. Hubschle, C. B.; Sheldrick, G. M.; Dittrich, B., ShelXle: a Qt graphical user interface for SHELXL. *J Appl Crystallogr* **2011**, *44* (Pt 6), 1281-1284.
- 29. Izumi, F.; Momma, K., Three-Dimensional Visualization in Powder Diffraction. *Solid State Phenomena* **2007**, *130*, 15-20.
- 30. Blochl, P. E., Projector augmented-wave method. *Phys Rev B Condens Matter* **1994,** *50* (24), 17953-17979.
- 31. Kresse, G.; Joubert, D., From ultrasoft pseudopotentials to the projector augmented-wave method. *Physical Review B* **1999**, *59* (3), 1758-1775.
- 32. Kresse, G.; Hafner, J., Ab initio molecular dynamics for liquid metals. *Phys Rev B Condens Matter* **1993**, *47* (1), 558-561.
- 33. Kresse, G.; Furthmüller, J., Efficiency of ab-initio total energy calculations for metals and semiconductors using a plane-wave basis set. *Computational Materials Science* **1996**, *6* (1), 15-50.
- 34. Kresse, G.; Furthmuller, J., Efficient iterative schemes for ab initio total-energy calculations using a plane-wave basis set. *Phys Rev B Condens Matter* **1996**, *54* (16), 11169-11186.
- 35. Perdew, J. P.; Ruzsinszky, A.; Csonka, G. I.; Vydrov, O. A.; Scuseria, G. E.; Constantin, L. A.; Zhou, X.; Burke, K., Restoring the density-gradient expansion for exchange in solids and surfaces. *Phys Rev Lett* **2008**, *100* (13), 136406.
- 36. Shannon, R. D., Revised effective ionic radii and systematic studies of interatomic distances in halides and chalcogenides. *Acta Crystallographica Section A* **1976**, *32* (5), 751-767.
- 37. Brese, N. E.; O'Keeffe, M., Bond-valence parameters for solids. *Acta Crystallographica Section B Structural Science* **1991**, *47* (2), 192-197.
- 38. Krebs, B.; Wallstab, H.-J., Thio-hydroxoanionen des Germaniums: Darstellung, Struktur und Eigenschaften von Na2GeS2(OH)2 \cdot 5 H2O / Thio-hydroxo Anions of Germanium: Preparation, Structure and Properties of Na2GeS2(OH)2 \cdot 5 H2O. *Zeitschrift für Naturforschung B* **1981**, *36* (11), 1400-1406.

- 39. Berastegui, P.; Hull, S.; Garcı Garcı, F. J.; Grins, J., A Structural Investigation of La2(GeO4)O and Alkaline-Earth-Doped La9.33(GeO4)6O2. *Journal of Solid State Chemistry* **2002**, *168* (1), 294-305.
- 40. León-Reina, L.; Losilla, E. R.; Martínez-Lara, M.; Bruque, S.; Aranda, M. A. G., Interstitial oxygen conduction in lanthanum oxy-apatite electrolytes. *J. Mater. Chem.* **2004**, *14* (7), 1142-1149.
- 41. <Kubelka-1931-Ein Beitrag Zur Optik Der Farbans.pdf>.
- 42. Broadley, S.; Gal, Z. A.; Cora, F.; Smura, C. F.; Clarke, S. J., Vertex-linked ZnO2S2 tetrahedra in the oxysulfide BaZnOS: a new coordination environment for zinc in a condensed solid. *Inorg Chem* **2005**, *44* (24), 9092-6.
- 43. Inaguma, Y., Lithium ion conductivity in the perovskite-type LiTaO3-SrTiO3 solid solution. *Solid State Ionics* **1995**, *79*, 91-97.

TOC figure

